Earth Planet. Sci. Lett. 690 (2026) 120180

Contents lists available at ScienceDirect

Earth and Planetary Science Letters

journal homepage: www.elsevier.com/locate/epsl

Evaluating the roles of alkalinity, evaporation, and basin hydrology in phosphorite deposition

Chenyi Tu [a,b,*], Jana Meixnerova [b,c], Brett Smith [c], Eva E. Stüeken [b,d], Roger Buick [b,c], Christopher J. Tino [e], Michael A. Kipp [a,b,*]

[a] Division of Earth & Climate Sciences, Nicholas School of the Environment, Duke University, Durham 27708, NC, USA
[b] Virtual Planetary Laboratory, NASA Nexus for Exoplanet Systems Science, USA
[c] Department of Earth & Space Sciences, University of Washington, Seattle 98195, WA, USA
[d] School of Earth & Environmental Sciences, University of St. Andrews, St Andrews, Fife KY16, 9AL, Scotland, UK
[e] Department of Earth, Energy, and Environment, University of Calgary, Calgary T2N 1N4, AB, Canada

ARTICLE INFO

Editor: Dr Tristan Horner

Keywords:
Phosphorites
Phosphorus
Nitrogen cycling
Alkalinity
Basin restriction

ABSTRACT

Phosphorus, an essential element for all forms of life, is recognized as the ultimate limiting nutrient controlling marine primary production over geological timescales. Phosphorites, which are the most phosphorus-rich sedimentary deposits, therefore serve as a valuable archive for reconstructing past marine phosphorus cycling. However, the origin of ancient phosphorites—whether their occurrences reflect changes in the global seawater nutrient inventory or are instead tied to local depositional conditions—remains debated. To shed light on this question, we examined the Permian Phosphoria Formation, a phosphorus-rich sequence deposited along western Pangaea. While previous models attribute extensive phosphogenesis to open ocean upwelling along a continental margin as in modern analogs, trace element concentration data suggest that Phosphoria environments were instead (semi)-restricted. Notably, bulk sediments exhibit exceptionally high $\delta^{15}N$ values ($> +15‰$). This may result from NH_3 volatilization, implying unique local water mass chemistry with elevated pH and alkalinity. Alkaline conditions, further enhanced by vigorous evaporation, could have promoted phosphate accumulation in the water column. We propose an alternating redox model to explain the observed pattern of phosphate enrichment in the sediments. Our study highlights the importance of local factors—specifically alkalinity, evaporation, and basin restriction—in driving phosphogenesis in the Phosphoria Formation, with implications for other phosphorus-rich successions in deep time. These insights may help illuminate the temporal clustering of phosphorites in the geologic record, specifically during the early and late stages of the Proterozoic.

1. Introduction

Phosphorus (P), an essential nutrient, is widely considered to control the rate of primary productivity in the oceans over geological timescales (Tyrrell, 1999). Consequently, the evolution of the marine P cycle may have played a key role in shaping ocean-atmosphere oxygen levels, alongside major episodes of biospheric innovation and radiation throughout Earth's four-billion-year history (Reinhard et al., 2017). Reconstructing past marine P cycling is therefore critical and often relies on geochemical signatures preserved in ancient sedimentary rocks, including fine-grained siliciclastic sediments (Reinhard et al., 2017) and chemical precipitates such as banded iron formations (Bjerrum and Canfield, 2002) and carbonate rocks (Ingalls et al., 2022). Among these, phosphorites—exceptionally P-rich sedimentary rocks (i.e., rich in phosphate minerals such as apatite)—stand out as an end-member archive of past P cycling.

Phosphorites are P-rich sedimentary rocks that are often defined by a threshold P content (e.g., 18 wt% P_2O_5; Glenn et al., 1994); here we use the term more generally to refer to sedimentary rocks with at least several wt% P_2O_5. Phosphorites are commonly interbedded with shales, limestones, dolomites, and cherts, and display a variety of sedimentary textures, such as peloids, ooids, and clasts. Despite forming in a range of lithological settings, they share some consistent characteristics. Phosphorite deposition is frequently linked to shallow (Bushinski, 1964), sediment-starved environments (Föllmi, 2016)—at least during the primary precipitation of apatite, although phosphatic particles can be

* Corresponding authors at: Division of Earth & Climate Sciences, Nicholas School of the Environment, Duke University, Durham 27708, NC, USA.
E-mail addresses: chenyi.tu@duke.edu (C. Tu), michael.kipp@duke.edu (M.A. Kipp).

https://doi.org/10.1016/j.epsl.2026.120180
Received 6 December 2025; Received in revised form 4 June 2026; Accepted 10 June 2026
Available online 17 June 2026

re-worked and transported to deeper settings (Föllmi et al., 1992). Phosphorus-rich rocks are also commonly found in association with stromatolites within the same stratigraphic successions (e.g., Southgate, 1980), and with evaporitic deposits within the same depositional basins (Hite, 1978). Additionally, detailed examinations of modern phosphorites suggest that their formation is influenced by sea-level fluctuations, with maximum P enrichment typically occurring during marine transgressions (Pufahl and Groat, 2017). This pattern aligns with the commonly observed association between P enrichment and carbonate hardgrounds (Christ et al., 2015).

Despite these known sedimentological relationships, the depositional environments that gave rise to ancient phosphorites remain poorly constrained, leaving open debates about the dominant controls on phosphorite prevalence through Earth history. Specifically, some have argued that phosphorite occurrences reflect changes in the global seawater nutrient inventory (Papineau et al., 2010), while others have highlighted the importance of local depositional conditions (Filippelli and Delaney, 1992). In the geological record, phosphorites are globally distributed during two notable intervals: the Paleoproterozoic and the Neoproterozoic-Cambrian transition. Both periods were marked by tectonic reorganization (i.e., supercontinent breakup) and global biogeochemical perturbations, particularly in the oxygen and carbon cycles (reviewed in Papineau et al., 2010). This temporal coincidence has led authors to infer potential cause-and-effect relationships between widespread phosphogenesis and the coeval Earth-system changes. For example, some models link the formation of Paleoproterozoic phosphorites to intensified continental weathering and the resulting increase in P flux to the oceans—an input that may have stimulated marine primary productivity, enhanced organic carbon burial, and ultimately contributed to atmospheric oxygenation (Papineau et al., 2010). However, some P-rich sedimentary successions in Earth history exhibit anomalous geochemical signatures—such as unusually heavy nitrogen ($\delta^{15}N$) (e.g., Papineau et al., 2009; Keighley, 2015) and inorganic carbon ($\delta^{13}C$) isotopic ratios (e.g., Papineau et al., 2013) —that are difficult to reconcile with global marine signals. The anomalies suggest that phosphorite formation in these cases may have been driven by localized water mass chemistry within hydrologically restricted basins, rather than by secular changes in global marine nutrient levels.

Recently, a growing body of studies indicate that elevated $\delta^{15}N$ values in ancient rocks (as noted above) may reflect high pH and alkalinity (carbonate-rich) in local aquatic environments (e.g., Stüeken et al., 2015, 2020; Velazquez et al., 2025). Such conditions, analogous to those in modern alkaline systems, are known to promote phosphate (PO_4^{3-}) accumulation via titration of calcium (Ca) from the water column via calcium carbonate precipitation, which leaves apatite undersaturated even at millimolar-range PO_4^{3-} concentrations (Toner and Catling, 2020; Haas et al., 2025). If the accumulated water-column PO_4^{3-} reservoir were subject to rapid precipitation (e.g., following an influx of Ca or drop in alkalinity that would promote apatite crystallization), this could lead to P enrichment in sediments. Based on this framework, we hypothesize that many phosphate deposits in the geological past could have been associated with hydrologically restricted settings, where phosphogenesis was primarily controlled by local factors such as elevated alkalinity. For instance, the Eocene Green River Formation, which was deposited in evaporitic lakes, contains co-occurring alkali minerals (i.e., trona and nahcolite), elevated $\delta^{15}N$ signatures, and

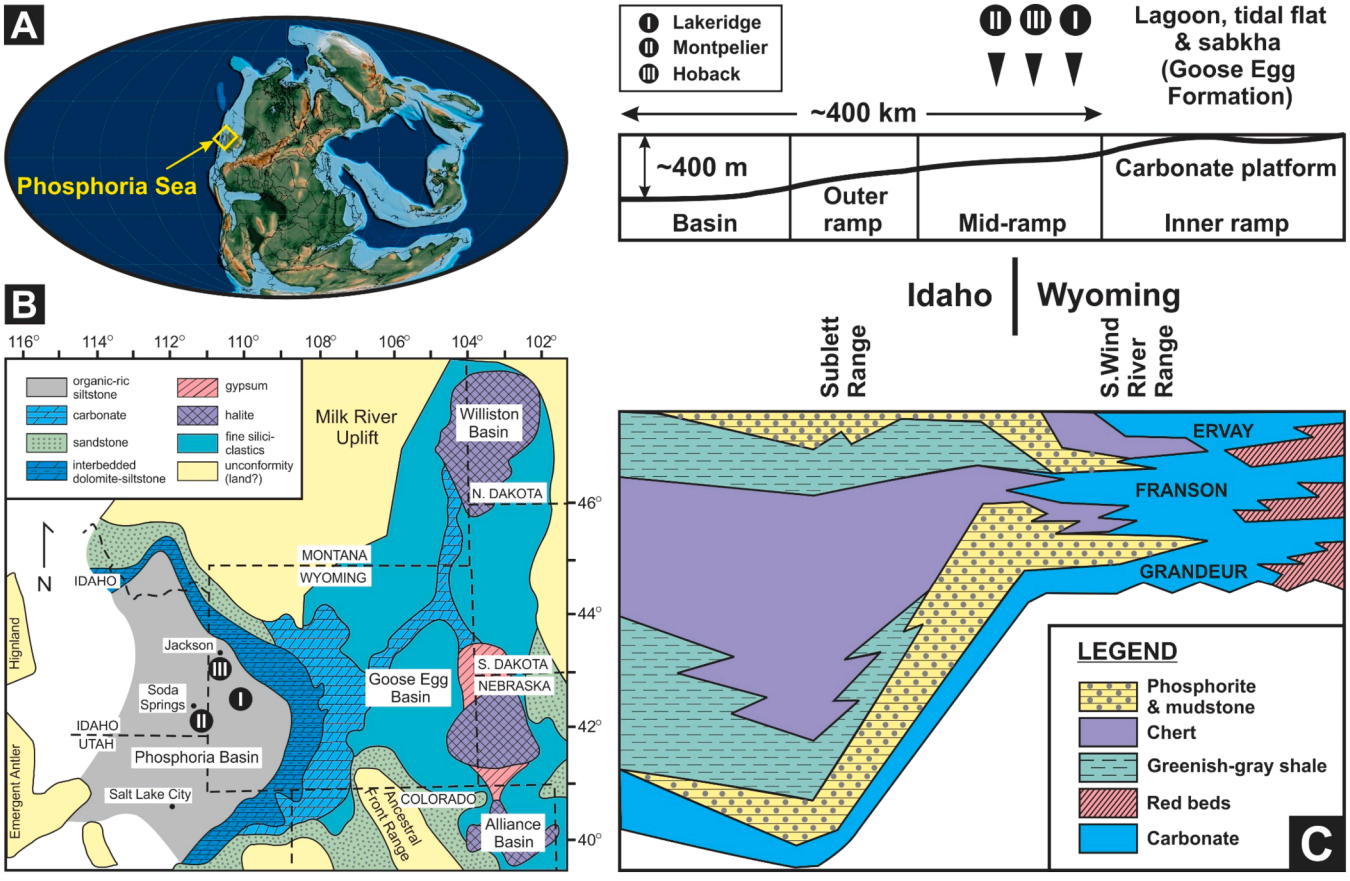

Fig. 1. Geological setting of the Phosphoria Basin and depositional environments of the studied sections in western United States. (A) Middle–Late Permian global paleogeographic map (from Scotese, 2021) highlighting the position of the Phosphoria Sea. (B) Geological map of the Phosphoria Basin, with coeval evaporite deposits and redbeds in the adjacent Goose Egg Basin to the east, modified from Maughan (1994). (C) Depositional settings of the studied sections, with the generalized lithological relationships of the Phosphoria Formation and the Park City Formation (consisting of three carbonate-dominated members—the Grandeur, Franson, and Ervay), modified from Perkins et al. (2003). Note that I, II, and III represent Lakeridge, Montpelier, and Hoback, respectively.

episodic P enrichments (Collister and Hays, 1973; Keighley, 2015; Lowenstein et al., 2017), consistent with this hypothesis.

To evaluate the applicability of this model—that phosphorus enrichments are primarily governed by local depositional conditions—to more ancient, massive phosphate deposits, we focus on the Permian Phosphoria Formation, which is a P-rich sedimentary sequence deposited within a subtropical epicontinental sea (the "Phosphoria Sea") along the western margin of Pangaea (Fig. 1A). This unit represents one of the world's largest known phosphatic rock resources, containing an estimated five to six times the total amount of P present in today's oceans (Sheldon, 1989). In the P-rich beds, peloids and coated grains (i.e., francolite) are the dominant components of the facies and are interpreted to have formed through authigenic phosphogenesis (Matheson and Frank, 2020). Some granular phosphorites may reflect reworking; however, these P-rich rocks are generally considered to represent in situ precipitation, as indicated by their poor sorting (Matheson and Frank, 2020). Notably, this extensive P-rich system has no direct modern depositional analog and the cause of the extensive phosphogenesis remains elusive. Most models propose an upwelling system along the western margin of Pangaea, invoking cold, nutrient-rich deep waters, analogous to modern settings such as the Peruvian shelf margin (e.g., McKelvey et al., 1959; Hein et al., 2004). These models implicitly assume that the depositional environments were well connected to the coeval open ocean. However, the Phosphoria Sea was at least partially isolated from the open Panthalassa Ocean by a remnant of the Antler Highland (Geslin et al., 1998), and bordered to the east by arid, highly evaporative sabkha environments (Fig. 1B, see more details in Section 2). These conditions suggest that the P-rich sequence may instead reflect deposition in a semi-restricted setting, where local factors could have played a significant, if not dominant, role in phosphogenesis.

Here, we examine one drill core (Lakeridge) from western Wyoming and two outcrop sections (Montpelier and Hoback) located near the Idaho–Wyoming boundary (Fig. 1B). Specifically, the Lakeridge core captures a nearly continuous succession of the Phosphoria Formation. In contrast, the two outcrop sections are less complete but still capture the representative P-rich intervals. We employ bulk nitrogen isotopes ($\delta^{15}N_{bulk}$)—an emerging proxy for reconstructing aqueous pH and, by extension, alkalinity in ancient environments—to test the potential link between phosphorus enrichment and alkalinity. Combined with major and trace element analyses, this approach allows us to constrain the hydrological and chemical characteristics of the Phosphoria Basin. While our focus is on the Phosphoria Formation, the insights from this study extend to phosphogenesis in other P-rich sequences throughout Earth history, particularly those deposited during the Paleoproterozoic and the Neoproterozoic-Cambrian transition. Our study also has implications for astrobiology. Phosphorus is an essential component of information-encoding polymers and plays critical roles in cell structure and metabolism; it is therefore considered central to the origin of life on Earth and potentially on other habitable worlds (Westheimer, 1987). Identifying environmental conditions that sustain aqueous P availability is thus crucial. Our results extend prior work (e.g., Toner and Catling, 2020) which suggests that localized, alkaline environments may represent one such setting.

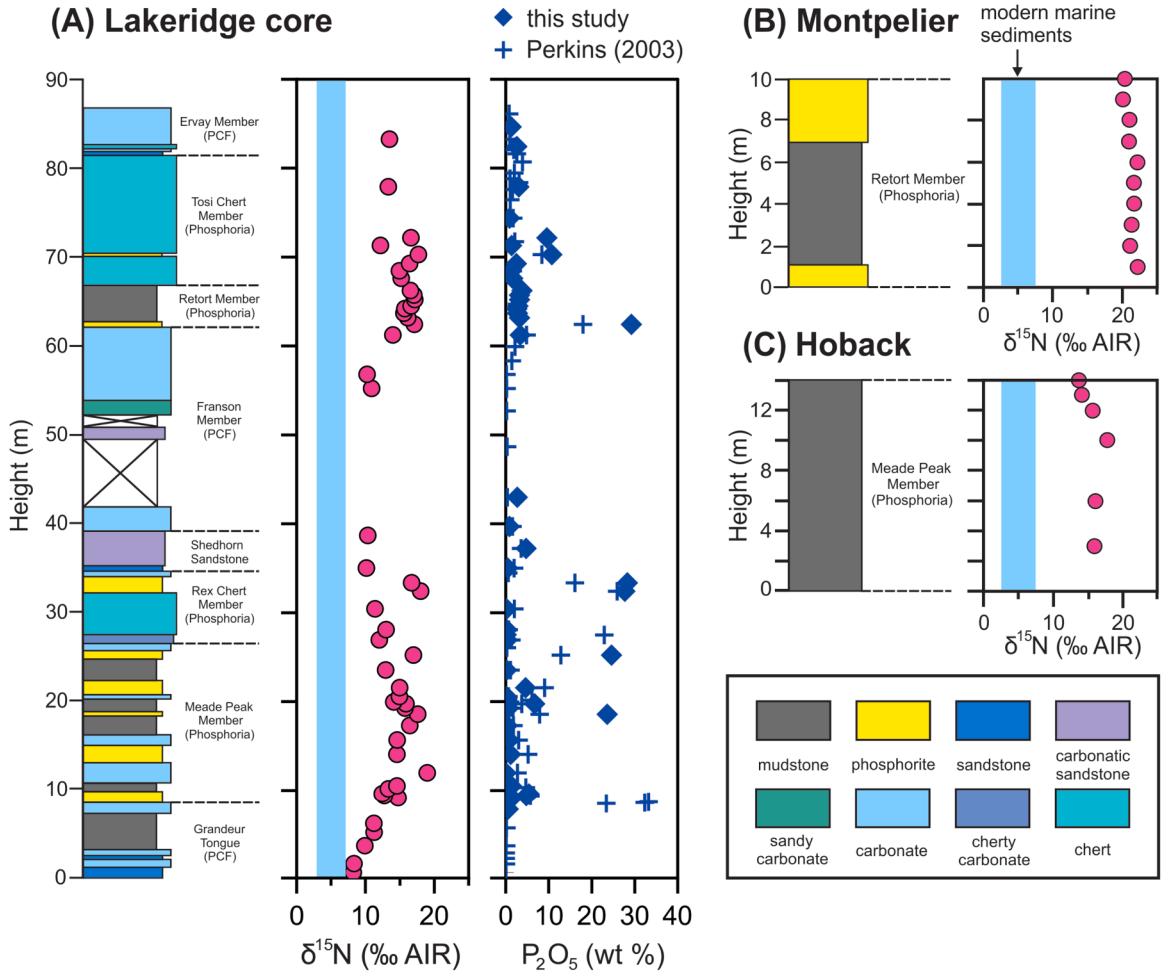

Fig. 2. Nitrogen isotope and phosphorus concentration data of the studied sections. (A) Lakeridge core. Some P_2O_5 concentration data are from Perkins et al. (2003). PCF = Park City Formation. (B) Montpelier. (C) Hoback. Blue shading represents the typical $\delta^{15}N$ values of the modern marine sediments.

2. Geological background and materials

The well-known Phosphoria Formation was deposited over a vast area of the present day western United States, spanning approximately 350,000 km^2 across Idaho, Wyoming, Montana, Utah, and Nevada (Hein et al., 2004; Fig. 1B). It comprises diverse lithologies, including phosphorites, cherts, and organic-rich mudstones (Fig. 1C and 2A), with P-rich beds primarily concentrated in the Meade Peak and Retort members (Fig. 2A). Overall, this succession was deposited on a low-gradient, westward-facing carbonate ramp (<200 m; Perkins et al., 2003), with phosphogenesis taking place both in basinal settings and shallower, inner-ramp environments (Fig. 1C; reviewed in Hein et al., 2004). Two depositional age models have been proposed: one constraining sedimentation from the latest Kungurian to the end of the Wordian (Wardlaw, 2015), and another extending deposition to the Permian–Triassic boundary (Davydov et al., 2018). In addition to the Phosphoria Formation, other sedimentary sequences also accumulated in the Phosphoria Sea, including shallow-marine siliciclastics (sandstones of the Shedhorn Formation) shed from the Milk River Uplift to the north, carbonates (the Park City Formation) and evaporitic deposits (the Goose Egg Formation) that are located in the desert to the east (Fig. 1B, C; reviewed in Hein et al., 2004). Although each formation was deposited primarily within specific portions of the basin, tongues of some units extend considerable distances (McKelvey et al., 1959). For instance, carbonate- and evaporite-dominated deposits in the eastern basin occasionally contain tongues of the Phosphoria Formation (Fig. 1C).

The Lakeridge core (~90 m) was recovered from General Petroleum's Lakeridge No. 43–19-G well in Sublette County, Wyoming (western United States, Fig. 1B). Now archived at the U.S. Geological Survey core repository in Lakewood, Colorado, this core captures a nearly complete and unweathered succession of Middle–Late Permian strata. Within it, the Phosphoria Formation intertongues with carbonate rocks of the Park City Formation (Fig. 1C). The Phosphoria Formation is divided into two depositional sequences. The lower sequence, comprising the Meade Peak phosphatic shale and Rex Chert Members, is generally considered to lie unconformably on the sandy carbonates of the Grandeur Tongue of the Park City Formation (Fig. 2A). The carbonate-rich Franson Member of the Park City Formation—as a basinward-projecting tongue—overlies the lower Phosphoria sequence (Fig. 1C). Above the carbonates lies the upper Phosphoria sequence, consisting of the Retort phosphatic shale and Tosi Chert Members, which is further overlain by the carbonate-rich Ervay Member of the Park City Formation (Fig. 2A). Several intervals of carbonate-rich quartz sand, referred to as the Shedhorn Sandstone, are also present within the Lakeridge core (Fig. 2A). Further details are provided in Perkins et al. (2003). In addition to the core, we also collected samples from two outcrop sections near the Idaho–Wyoming border: Montpelier, ID (~10 m) and Hoback Junction, WY (~14 m) (Fig. 1B). These sections capture the Retort Member and the Meade Peak Member of the Phosphoria Formation, respectively (Fig. 2B, C). In terms of sedimentary environments, previous studies suggest that the Lakeridge core represents a mid- to inner-ramp depositional setting that might have been influenced by storm-induced wave-base turbulence (Perkins et al., 2003). The Montpelier and Hoback sections, situated in close proximity to the Lakeridge core, are interpreted to record similar depositional environments, although the Montpelier section appears to have been slightly more distal from sediment sources.

3. Methods

Any visible veins or weathered surfaces were removed from samples with a water-cooled rock saw, and the remaining portions were hammered or cut into small pieces and thoroughly rinsed with deionized (DI) water. Next, a shatterbox with an alumina (ceramic) puck was used to produce homogenized powders. All N isotopic analyses (bulk and kerogen-bound) were performed at the University of Washington. For bulk $\delta^{15}N$ analyses, the rock powders were decarbonated via two treatments with 2 M HCl at 60 °C overnight. The residues were then rinsed three times with 18 megaohm DI water and dried in an oven. Following this, the sample powders were weighed into tin capsules (8 × 5 mm) and analyzed with a Costech ECS 4010 Elemental Analyzer coupled to a Thermo MAT253 Isotope Ratio Mass Spectrometer. Isotopic ratios are expressed as $\delta = (R_{sample}/R_{standard} - 1) \times 1000$, where R is the ratio of $^{15}N/^{14}N$ (reported as $\delta^{15}N$). Nitrogen isotope data are reported relative to air as the isotopic standard. Sample data were cast on the $\delta^{15}N_{air}$ scale via two-point calibration using in-house standards (two glutamic acids and dried salmon powder; Kipp et al., 2018) that are calibrated to the international reference materials USGS40 and USGS41. Replicate analyses of USGS Green River Shale (SGR-1) were used to demonstrate analytical reproducibility, particularly at the high end of the $\delta^{15}N$ scale, yielding an average value of $\delta^{15}N = +18.1 \pm 0.5‰$).

Kerogen isolation was performed as in Kipp et al. (2018). Homogenized rock powders were weighed into fluoropolymer bottles and treated with 50% v/v (~15 M) hydrofluoric acid (HF) overnight in a shaking water bath at 55 °C. The resulting solutions were centrifuged and the supernatant (containing dissolved silicate phases) was decanted. The residual phase was treated with 62.5 g H_3BO_3 dissolved in 50% HF to produce BF_3 to remove residual fluoride phases formed by excess HF. Samples were centrifuged, the supernatant again decanted, and the samples were rinsed three times with DI–H_2O. The kerogen was transferred to a glass vial in DI–H_2O and freeze-dried to remove moisture prior to analysis. Kerogen isotopic analyses followed the same protocol as bulk samples. Aliquots of kerogen were analyzed for C/H ratios on a CEC 440HA Elemental Analyzer in the Marine Analytical Laboratory at University of California Santa Barbara.

Major and trace element concentrations were determined via X-ray fluorescence (XRF) and ICP-MS, respectively at ALS Geochemistry, and also compiled from Perkins et al. (2003) for the Lakeridge Core. Ce anomalies (Ce/Ce^*_{SN}) and Pr anomalies (Pr/Pr^*_{SN}) are calculated here based on their relative enrichments or depletions (normalized to the Post-Archean Australian Shale—PAAS) compared with neighboring REEs: $Ce/Ce^*_{SN} = Ce_{SN} \times Nd_{SN}/(Pr_{SN})^2$ and $Pr/Pr^*_{SN} = Pr_{SN}/(0.5Ce_{SN} + 0.5Nd_{SN})$.

4. Results

The Lakeridge drill core contains multiple P-enriched horizons, reaching 25–30% P_2O_5, primarily within the Meade Peak and Retort members (Fig. 2A). From the base of the core, $\delta^{15}N_{bulk}$ values increase gradually over ~10 m, from about +8‰ to a maximum of +19‰, and then remain generally elevated. Toward the base of the Shedhorn Sandstone (at ~35 m depth), values decline slightly to ~+10‰ (Fig. 2A). In the upper portion of the core, $\delta^{15}N_{bulk}$ shows a second increasing trend, from ~+11‰ to a peak of +18‰ within the Retort Member, and then remains generally high (Fig. 2A). Overall, relatively elevated $\delta^{15}N_{bulk}$ values coincide with intervals of maximum P enrichment. Additionally, $\delta^{15}N_{bulk}$ from the two outcrop sections, Montpelier and Hoback, are consistently high, with mean values of +21.2 ± 0.7‰ and +15.5 ± 1.4‰, respectively (Fig. 2B, C). For all the three locations, the total nitrogen (TN) content broadly covaries with the corresponding total organic carbon (TOC) concentration (Fig. S1A), implying that the majority of nitrogen is derived from marine organic matter, despite subsequent remineralization in the water column and during early diagenesis following burial.

In addition to bulk $\delta^{15}N$ measurements, we analyzed nitrogen concentrations and isotope ratios of kerogen-bound N ($\delta^{15}N_{kerogen}$) in six representative samples—five from the Lakeridge core and one from the outcrop (Hoback). Their carbon-to-nitrogen (C/N) and carbon-to-hydrogen (C/H) molar ratios range from 38.6 to 59.1 and 1.9 to 2.4, respectively (Table S1). The $\delta^{15}N_{kerogen}$ values closely match the corresponding $\delta^{15}N_{bulk}$ values to within 0.2–0.9‰ except for one sample

(Table S1).

We also measured trace element concentrations in samples from the Lakeridge drill core. Several samples from the lowermost interval show elevated molybdenum (Mo) contents, reaching up to ~160 ppm, whereas the remaining samples display comparatively low concentrations, with an average of 8.7 ± 8.8 ppm (Fig. 3). Uranium (U) concentrations are notably higher (50–100 ppm; Fig. 3) in samples enriched in phosphorus (P_2O_5 >20 wt%), consistent with the role of apatite as an important U sink (Altschuler et al., 1958). In contrast, P-poor samples contain low U concentrations, averaging 6.9 ± 7.7 ppm (Fig. 3). The five phosphorite samples (P_2O_5 >20 wt%) also exhibit pronounced shale-normalized (SN) negative cerium anomalies (Ce/Ce^*_{SN}), with an average of 0.24 ± 0.04 (Fig. 4). The full dataset is provided in the Supplementary Data.

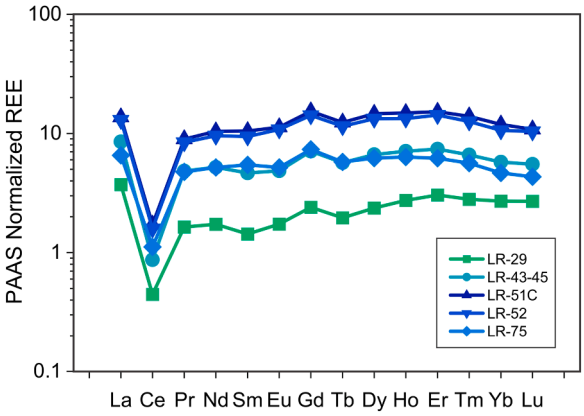

Fig. 4. Distribution patterns of the REE concentrations (shale-normalized) of the phosphorite samples (with P_2O_5 >20 wt%) within the Lakeridge drill core.

5. Discussion

5.1. Hydrological and chemical characteristics of the Phosphoria Basin

We first aim to characterize the hydrological and chemical properties of the Phosphoria Basin. Most samples from the Lakeridge drill core contain relatively low iron concentrations (<0.5%), which precludes the use of iron speciation as a reliable proxy for reconstructing water-column chemistry (Raiswell et al., 2018). Instead, we focus on redox-sensitive trace metals and TOC concentrations to infer the first-order redox conditions within the basin. The burial rates of both trace metals and organic carbon are typically elevated in sediments deposited beneath reducing and/or euxinic (sulfide-rich) bottom waters compared to those underlying well-oxygenated seawater (e.g., Bennett and Canfield, 2020). As a result, their enrichments archived in ancient rocks can provide insights into the local (and potentially global) marine redox dynamics (e.g., Sahoo e al., 2023).

Our drill core samples are generally characterized by relatively low TOC (<1.0 wt%) and muted concentrations of redox-sensitive trace metals (Mo and U), except in the lower portion of the section and in P-rich samples for U specifically (Fig. 3). This pattern suggests that most sediments were deposited beneath oxic to non-euxinic reducing bottom waters (Bennett and Canfield, 2020), consistent with the generally low organic carbon/total phosphorus ratios (C_{org}/P) observed in our samples (Fig. S2) (Algeo and Ingall, 2007). By contrast, several samples from the lower part of the section (at ~10 m height) exhibit markedly higher Mo concentrations relative to the rest of the succession (Fig. 3). Unlike many other trace metals, Mo sequestration is highly sensitive to euxinic conditions, where removal from seawater is strongly enhanced relative to both oxygenated and non-euxinic reducing environments (Scott and Lyons, 2012). The substantially elevated Mo concentrations observed in several samples (note that these are not the P-rich samples, which were instead tied to well-ventilated conditions, see Section 5.3) therefore suggest intervals of at least transient euxinia within the Phosphoria

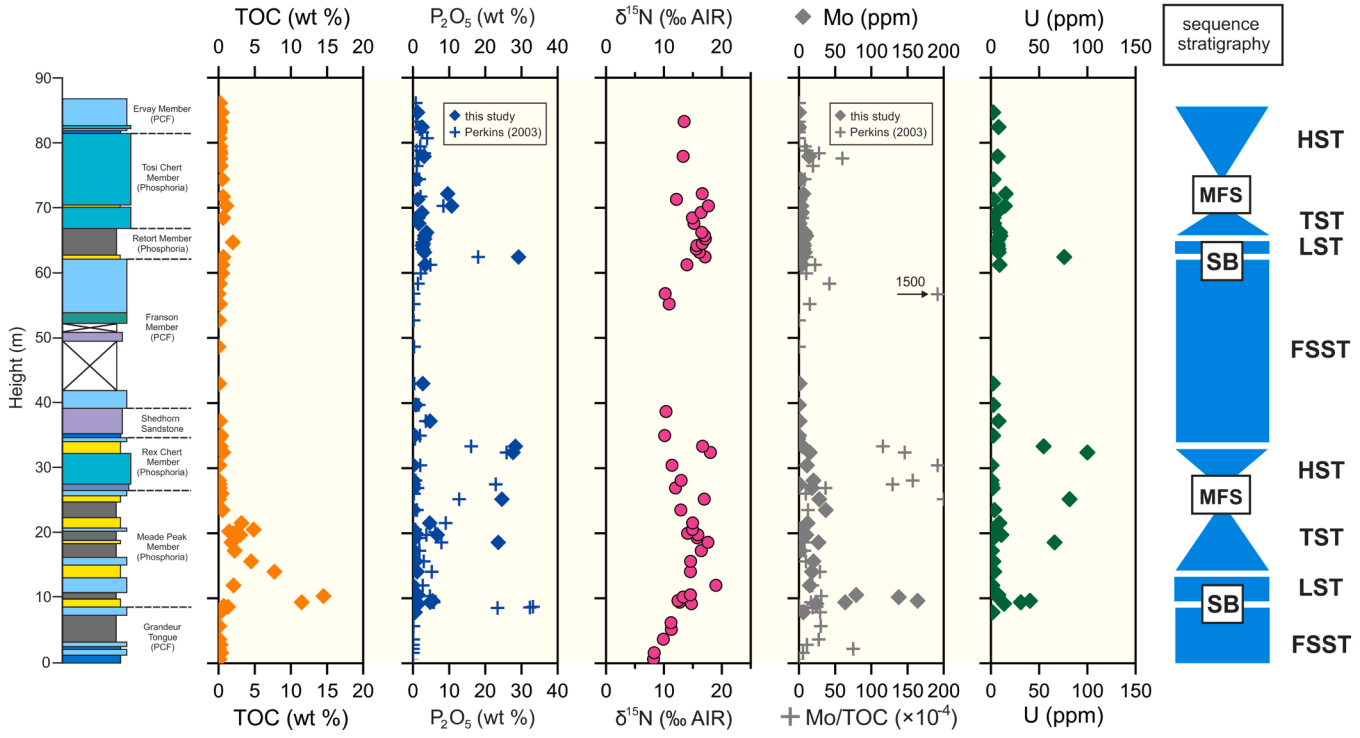

Fig. 3. Integrated geochemical profiles of the Lakeridge drill core. Data include TOC concentrations (from Perkins et al. (2003)), P_2O_5 contents (some data are from Perkins et al. (2003)), nitrogen isotopes, Mo and U concentrations (Mo/TOC ratios are calculated based on data from Perkins et al. (2003)). The sequence stratigraphic model is taken from Hiatt (1997). Note that SB = sequence boundary, MFS = maximum flooding surface, FSST = falling stage systems tract, LST = lowstand systems tract, TST = transgressive systems tract, HST = highstand systems tract. PCF = Park City Formation.

Basin.

In sulfide-rich settings, sedimentary Mo/TOC ratios can be further used to constrain hydrological conditions, specifically the degree of water-mass restriction. Detailed studies on modern restricted basins show that increasing restriction is closely correlated with systematically lower Mo/TOC ratios recorded in sediments (Algeo and Lyons, 2006). Two processes lead to these muted values in highly restricted settings (<10 for the Black Sea and Framvaren Fjord): (1) rapid Mo drawdown from the water column, and (2) limited seawater renewal from the open ocean, which would otherwise replenish the basin's Mo reservoir. In general, our samples from the euxinic interval exhibit relatively low Mo/TOC ratios (<30), comparable to those of the modern Cariaco Basin (25 ± 5), and lower than those of the euxinic settings that are more connected to the modern ocean (45 ± 5 for Saanich Inlet) (Algeo and Lyons, 2006). Assuming a similar marine Mo inventory in the Permian ocean as today (Dahl et al., 2010), this would suggest that the Phosphoria Basin was at least semi-restricted, with limited connection with the global ocean along its western margin. Such hydrological restriction is consistent with the paleogeographic configuration of the Phosphoria Sea, which was partially separated from the Panthalassa Ocean by the remnant Antler Highland (Geslin et al., 1998). Further support comes from strontium isotope data from carbonates within the Phosphoria Formation ($^{87}Sr/^{86}Sr$ = 0.7076–0.7086), which are more radiogenic than the coeval isotopic composition of the global ocean ($^{87}Sr/^{86}Sr$ = 0.7068–0.7070) (Hill et al., 2024), thus reflecting local continental weathering signatures and reinforcing the argument that the Phosphoria Basin was indeed somewhat restricted.

Moreover, multiple lines of evidence indicate that water masses within the Phosphoria Basin were more saline than normal seawater. First, dolomites and extensive evaporite deposits—including anhydrite and halite—occur within the Phosphoria Basin and adjacent basins to the east (Fig. 1B; Stephens and Carroll, 1999; Hein et al., 2004). These facies formed contemporaneously with the P-rich successions of the Phosphoria Formation, suggesting that the phosphogenesis also took place under arid, highly evaporative, and saline conditions. Climate simulations are consistent with this inference, indicating that the western margin of Pangaea experienced low precipitation during the Middle–Late Permian (Li et al., 2022). In addition to the evidence above, available geochemical data further corroborate such conditions. Oxygen isotope compositions from the coeval phosphorites record elevated shallow-water temperatures of 34–37 °C (Hiatt and Budd, 2001), while the contemporaneous landward carbonates (dolomites) display relatively high oxygen isotopic values [$\delta^{18}O = +(4–5)‰$], which are typical of evaporative conditions (Pommer and Sarg, 2018). Moreover, elevated concentrations of gammacerane reported from the Phosphoria Formation provide additional support for salinity stratification and the development of hypersaline waters within the basin (Stephens and Carroll, 1999).

5.2. Elevated alkalinity and its role in phosphate buildup in the water column

Interestingly, we find exceptionally high $\delta^{15}N_{bulk}$ values (>+15‰) in both drill core and outcrop samples (Fig. 2). These values are markedly higher than the global average for modern marine sediments (+5‰; Tesdal et al., 2013) and other Permian strata (+(4–6)‰; Algeo et al., 2014). Before evaluating possible environmental drivers of this trend, we first consider the potential effects of metamorphic overprinting on the nitrogen isotope compositions recorded in these ancient rocks. Numerous studies have shown that thermal alteration can elevate $\delta^{15}N$ and C/N values in both bulk rocks and the associated kerogen. The extent of the enrichment increases with metamorphic grade and arises from the preferential loss of ^{14}N (reviewed in Stüeken et al., 2016, see references therein). In our samples, generally low kerogen C/N ratios (40–60 mol/mol; Table S1), together with the absence of a correlation between bulk C/N ratios and $\delta^{15}N_{bulk}$ values (Fig. S1B), argue against significant metamorphic alteration. Similarly, C/H ratios of kerogen are a widely used proxy for assessing thermal maturation of biomass, since hydrogen is preferentially lost relative to carbon even at sub-greenschist grades (Hayes et al., 1983). The kerogen in our samples yields C/H ratios of ~2 (Table S1), consistent with a low metamorphic grade equivalent to the prehnite–pumpellyite facies (Hayes et al., 1983). Moreover, the lack of a positive correlation between C/H ratios and $\delta^{15}N_{kerogen}$ further corroborates relatively low thermal maturity (Fig. S1C). Under such low-grade conditions, bulk rock $\delta^{15}N$ values are typically enriched by <1‰ (Stüeken et al., 2017). Therefore, the exceptionally high $\delta^{15}N$ values archived in our samples most likely represent primary geochemical signatures.

Several mechanisms could be responsible for the elevated nitrogen isotope compositions observed in our samples. We first consider denitrification (reduction of dissolved NO_3^- to gaseous N_2), a process that is associated with large isotopic fractionation between product and reactant ($\varepsilon = \delta_{product} - \delta_{reactant} \approx -5$ to $-30‰$) (reviewed in Stüeken et al., 2016) and is thought to play the dominant role in setting the modern marine N isotope mass balance. Although sediments deposited in modern oxygen deficient zones are tied to enhanced denitrification and often exhibit relatively high $\delta^{15}N$, values exceeding +15‰ are rare (Tesdal et al., 2013). Additionally, our phosphorite samples yield remarkably negative Ce anomalies (Fig. 4), indicating well-ventilated water-column conditions (see Section 5.3, Tostevin, 2021). Such conditions would seem to be inconsistent with the widespread anoxia required to sustain high degrees of denitrification. Moreover, elevated salinity—such as that inferred for the Phosphoria Basin—can inhibit microbial nitrogen metabolisms, specifically nitrification and denitrification (e.g., Tino et al., 2025). Taken together, these factors indicate that denitrification alone may not be sufficient to explain the elevated $\delta^{15}N$ values.

We next consider partial nitrification ($\varepsilon \approx -1$ to $-25‰$; reviewed in Stüeken et al., 2016) and partial ammonium (NH_4^+) assimilation ($\varepsilon \approx -4$ to $-27‰$; reviewed in Stüeken et al., 2016). Both processes generate isotopically light products (nitrate or biomass), leaving behind residual NH_4^+ enriched in ^{15}N that could be assimilated elsewhere within the same basin. If these mechanisms dominated, we would expect pronounced isotopic heterogeneity, expressed as a wide range of $\delta^{15}N$ values in the sedimentary record. However, our samples yield consistently high nitrogen isotope compositions through time and across sites, thus ruling out these pathways.

We argue that a more parsimonious explanation for our data is volatilization of ammonia (NH_3) from the water column into the atmosphere. This process imparts a large isotope fractionation ($\varepsilon \approx -42‰$ at 25 °C, Li et al., 2012), leading to a uniform ^{15}N-enriched pool of residual NH_4^+ that can be subsequently assimilated into biomass. For this mechanism to operate, NH_4^+must dissociate to $H^+$and NH_3 in the water column. The yield of this reaction is governed by its pKa (the acid dissociation constant), which is 9.2 under standard temperature and pressure. Consequently, elevated $\delta^{15}N$ values (>+10‰) in sediments can be interpreted as a diagnostic signal of high pH—and thus elevated alkalinity—a relationship documented in both modern and ancient alkaline lake systems (e.g., Stüeken et al., 2015, 2020; Velazquez et al., 2025). We note that there is not necessarily a single threshold pH value at which $\delta^{15}N$ would become enriched, since NH_3 already comprises a few percent abundance at pH ~ 8. As discussed further below, the presence of a large NH_4^+ reservoir appears consistent with the hydrological and chemical conditions of the basin. Such a reservoir could have developed under both anoxic conditions (beneath a steep and shallow chemocline) and more oxygenated waters, provided salinity was high enough to inhibit microbial nitrification. The subsequent conversion of NH_4^+ to NH_3 would require relatively high pH—conditions that have important implications for P accumulation in the water column.

Modern alkaline lakes are notable for their high dissolved P levels, in stark contrast to the widespread P scarcity typical of most natural waters. This enrichment occurs because, in carbonate-rich environments, calcium is preferentially sequestered into carbonate minerals, thereby

inhibiting apatite precipitation as a major sink for PO_4^{3-}. Consequently, dissolved PO_4^{3-} can build up to exceptionally high concentrations—sometimes exceeding 10 mM (Toner and Catling, 2020; Haas et al., 2025). By analogy, we propose that elevated alkalinity in the Phosphoria Basin promoted PO_4^{3-} accumulation in the water column, a process that may have directly contributed to phosphogenesis (episodic P drawdown into sediments) in the Phosphoria Formation. This is supported by the observation that higher $\delta^{15}N$ values—and thus more elevated alkalinity—generally coincide with intervals of greater P enrichment, particularly in the Lakeridge drill core (Fig. 2A). Beyond the role of alkalinity, evaporation would have further facilitated PO_4^{3-} enrichment in the water bodies.

It is noteworthy that sodium-rich carbonate minerals (e.g., trona and nahcolite) are absent from our samples. These evaporite minerals are common in modern alkaline lakes and are occasionally observed in ancient systems with elevated pH (Keighley, 2015; Lowenstein et al., 2017). However, their extreme solubility and concomitant low preservation potential make them rare in deep-time records. Thus, their absence does not preclude the possibility of elevated pH in ancient aqueous systems. That said, the pH of the Phosphoria Basin was perhaps only moderately elevated relative to the coeval global ocean, given that the basin—though somewhat restricted—still received a moderate amount of seawater influx from the open ocean (see discussion below). Importantly, exceptionally high pH and alkalinity are not required to generate high nitrogen isotopic ratios in the NH_4^+ pool. In relatively shallow settings (<200 m) such as the Phosphoria Sea, mixing between the water column and atmosphere (e.g., during seasonal overturning) would have enhanced NH_3 degassing, leaving the residual NH_4^+ isotopically enriched. A similar mechanism has been invoked for loss of isotopically light volatile H_2S from the non-marine Green River Formation, which led to isotopic enrichment of the residual sulfate reservoir (Crémière et al., 2024; we also note that the Green River Formation exhibits elevated $\delta^{15}N$ up to +20‰ (Collister and Hays, 1973), consistent with NH_3 volatilization). In addition, intermittently anoxic conditions—indicated by trace metal enrichments and TOC concentrations (see Section 5.1)—would have promoted NH_4^+ buildup, facilitating NH_3 loss. Even during intervals with widespread oxic conditions (see Section 5.3), elevated salinity would have suppressed microbial nitrification (e.g., Tino et al., 2025), perhaps allowing NH_4^+ to accumulate in the water column. Collectively, these factors likely contributed to both the generation and preservation of the elevated $\delta^{15}N$ signatures.

One remaining question concerns the sources of alkalinity in the Phosphoria Basin. Evaporation of seawater alone cannot account for elevated alkalinity (Tosca and Tutolo, 2023), suggesting additional inputs. It is noteworthy that the Phosphoria Basin was bordered by the Milk River Uplift and the Ancestral Front Range (Fig. 1B), both of which are partly comprised of Precambrian basement rocks (igneous and metamorphic; Kluth and Coney, 1981; Shepard and Bartow, 1986). Weathering of these rocks, followed by riverine input, could have contributed to elevated alkalinity in the basin. Another potential source is the Antler Highland to the west (Fig. 1B), which contains mafic to intermediate rocks (basalt and andesite) emplaced by regional thrust faulting, although the timing of this emplacement remains uncertain (Late Permian to Early Triassic; Crafford, 2008). Additionally, inflows of carbonate-rich groundwater may have further enhanced basin alkalinity.

Next, we consider the source of P to the Phosphoria Basin. One possibility is enhanced continental runoff during this period. However, multiple studies suggest that terrestrial weathering intensity has remained relatively constant over geologic timescales, except during intervals of significant climatic perturbation (Lipp et al., 2021; Dzombak and Sheldon, 2022). This makes a dominant continental source of P less likely. Alternatively, an established framework of sequence stratigraphy indicates that the P-rich intervals of the Phosphoria Formation (the Retort and Meade Peak members) coincide with marine transgressions (Fig. 3) (Hiatt, 1997), a pattern also observed in many other ancient phosphorites (Pufahl and Groat, 2017). We therefore propose that incursions of open-ocean seawater replenished PO_4^{3-} in the basin, despite its semi-restricted nature. This is consistent with previous suggestions that upwelling from a nutrient-rich deep water source constituted the primary supply of P to the Phosphoria Formation (e.g., Hiatt, 1997; reviewed in Hein et al., 2004). Fossil evidence, namely the presence of cool-water brachiopods and conodonts, further supports periodic marine upwelling (Wardlaw, 2015).

Beyond these observations, we also examine trace metal patterns using the framework developed by Sweere et al. (2016). This approach distinguishes between two marine end-members: open-marine settings along continental margins and hydrographically restricted marginal basins. Notably, our samples (shales from the Meade Peak and Retort Members) are plotted within the "open/upwelling" field rather than the "restricted" field (Fig. S3). This pattern is consistent with a semi-isolated basin that intermittently received inputs of upwelled seawater from the coeval open ocean, rather than a fully restricted system analogous to the modern Black Sea, an interpretation that we consider unlikely. A caveat, however, is that the modern calibration dataset of Sweere et al. (2016) does not include an epeiric sea analogous to the Phosphoria Sea, which may limit the precision with which basin conditions can be constrained. Nevertheless, the available stratigraphic, paleontological, and geochemical evidence is mutually consistent in supporting intermittent exchange with the open ocean. Thus, while we emphasize the (semi-) restricted nature of the Phosphoria Basin, we argue that P was supplied to the basin from an external marine upwelling source, which was key to sustaining the P flux needed to fuel deposition of such a large phosphate deposit.

5.3. A "Phase-switch" model for phosphogenesis in the sediments

We also measured rare earth element (REE) concentrations in phosphorite samples from the Lakeridge drill core. The distribution of REEs in chemical precipitates can potentially provide a valuable fingerprint of the marine chemistry at the time of deposition (e.g., Tostevin et al., 2016; reviewed in Tostevin, 2021; Zhao et al., 2021). To achieve this goal, the first critical step is assessing potential diagenetic overprinting on the REE patterns. In general, the REE distributions of our samples exhibit a seawater-like rather than a flat or bell-shaped (i.e., middle REE-enriched) pattern (Fig. 4), suggesting diagenetic alteration and detrital contamination did not obscure the primary geochemical signals (Reynard et al., 1999; Zhao et al., 2021). This is further supported by the lack of a positive correlation between aluminum contents and total REE concentrations, which rules out significant detrital input (Fig. S4). Notably, our P-rich samples are characterized by significant negative Ce anomalies (Fig. 4), consistent with previous studies focusing on the Phosphoria Formation (e.g., Piper, 2001). In addition to the bulk rocks, data from specific mineral fractions—carbonate and apatite separated through sequential leaching (Hill et al., 2024)—also reveal distinct negative Ce anomalies (Fig. S5). It is noteworthy that these signatures could also arise from anomalous lanthanum (La) enrichment rather than true Ce depletion (Bau and Dulski, 1996). To distinguish these two scenarios, we followed the method of Bau and Dulski (1996) and detected shale-normalized positive praseodymium anomalies (Pr/Pr^*_{SN}) in our samples (Fig. S6). This confirms that the observed data reflect genuine negative Ce anomalies.

Cerium anomalies can shed light on local water column redox dynamics in Earth's deep past (e.g., Tostevin et al., 2016). Owing to its distinctive redox behavior, Ce(III) can be oxidized to insoluble Ce(IV) under oxygenated conditions. The resulting Ce(IV) is preferentially removed from solution as discrete oxide particles relative to the other REEs. This oxidation is commonly catalyzed on the surfaces of Mn (oxyhydr)oxides, where Ce oxides tend to accumulate. As a result, oxic settings become depleted in Ce and exhibit a negative Ce anomaly (Ce/Ce^*_{SN} <0.9). In contrast, under low-oxygen conditions, Mn (oxyhydr)oxides undergo reductive dissolution, releasing previously

sequestered Ce back into the water column. Thus, reducing water columns typically lack a negative Ce anomaly and may even display a positive anomaly (reviewed in Tostevin, 2021, see references therein). Given these constraints, we infer that the studied phosphorites were deposited under an oxygenated water column. This interpretation is supported by their general association with relatively low TOC concentrations (Fig. S7), and consistent with fossil records of abundant ichnofauna and benthic fauna (Marshall, 2025). By contrast, samples with low P contents are characterized by elevated TOC concentrations (Fig. S7), which may point to deposition under anoxic conditions.

We now synthesize the available lines of evidence discussed above. In terms of its physical characteristics, the Phosphoria Basin was marked by intense evaporation (as indicated by mineralogical features), elevated salinity (as indicated by evaporite occurrences, isotopic signatures, and biomarker evidence), and hydrological semi-restriction from the coeval open ocean (as indicated by sedimentological and trace metal constraints). Chemically, the basin was characterized by elevated alkalinity (as inferred from high $\delta^{15}N$ values) and dynamic redox conditions (as indicated by TOC, trace metal, and REE abundance data) that generally fluctuated between oxic and non-sulfidic reducing states. In addition, the basin episodically received PO_4^{3-} derived from marine upwelling in the open ocean. A key unresolved question is how this P inventory was transferred from the water column to the sediment and ultimately contributed to the extensive phosphate deposits of the Phosphoria Formation.

We propose a two-stage "phase-switch" model that integrates the diverse lines of evidence presented above into a coherent framework for phosphogenesis. The first stage is characterized by PO_4^{3-} buildup in the water column and relatively limited P burial in sediments. During periods of marine transgression, substantial PO_4^{3-} was supplied through upwelling from the open ocean into this (semi-)restricted basin. Elevated alkalinity, combined with evaporative concentration and Fe (II)-poor conditions (as indicated by low iron contents in the sediments; note that ferruginous conditions could promote phosphate sequestration; Derry, 2015), collectively enhanced PO_4^{3-} accumulation in the water column. Additionally, the relatively low Ca^{2+} concentration of Permian seawater, as inferred from diverse records including carbonate mineralogy (Sandberg, 1983), fluid inclusions (Lowenstein et al., 2001), and Ca isotopes in evaporites (Blättler and Higgins, 2014), may have further favored PO_4^{3-} enrichment in the Phosphoria Sea. This is because apatite is a primary sink for PO_4^{3-}, and under alkaline conditions dissolved Ca^{2+} would have first been sequestered in carbonate minerals, as discussed above. Elevated nutrient availability (i.e., P), in turn, fostered high productivity, marine anoxia, and enhanced organic matter burial (Fig. 5A). With the exception of the lowermost interval showing elevated Mo concentrations (see Section 5.1), the water column was likely oxygen-deficient but not strongly sulfidic. Under these conditions, P was gradually sequestered along with organic matter, rather than being recycled back into the water column as would be expected in euxinic settings (Ingall and Jahnke, 1994). This interpretation is consistent with the generally low C_{org}/P ratios observed in our samples (Fig. S2). As organic-bound P continued to settle and become buried, PO_4^{3-} concentrations in the water column—and thus primary productivity—would have declined, resulting in a more ventilated water column (the second stage; Fig. 5B). At the same time, P bound to previously buried organic matter could have been recycled (i.e., aerobic degradation) and precipitated as apatite within sediments. A key remaining question concerns the source of calcium (Ca) necessary for apatite formation. Based on the observation that certain P-rich intervals overlie carbonate layers (Fig. 3), we propose that some Ca in the porewaters may have been derived from partial dissolution of pre-existing carbonates, driven by pH decreases associated with the aerobic degradation of organic matter. An additional source of Ca could have been influxes of Ca-rich groundwater, which is plausible given that the studied sections are located relatively close to the eastern landmass (Fig. 1).

Interestingly, the carbonate fraction of the phosphorites exhibits relatively negative carbon isotope values (ranging from −3.1‰ to −10.8‰) (reviewed in Hein et al., 2004, see references therein), consistent with incorporation of authigenic carbon derived at least in part from the decay and recycling of buried organic matter. These observations support our proposed "phase-switch" scenario for phosphogenesis, which would be further facilitated by low detrital input, as reflected in muted aluminum contents in our samples (see data in Supplementary Data). In sum, our two-stage redox model helps explain the episodic nature of P enrichment in the studied sediments and may be applicable to other ancient P-rich successions. Notably, available data indicate that many phosphorite horizons are indeed associated with relatively low organic contents (Ilyin, 1998), congruent with the predictions of our model.

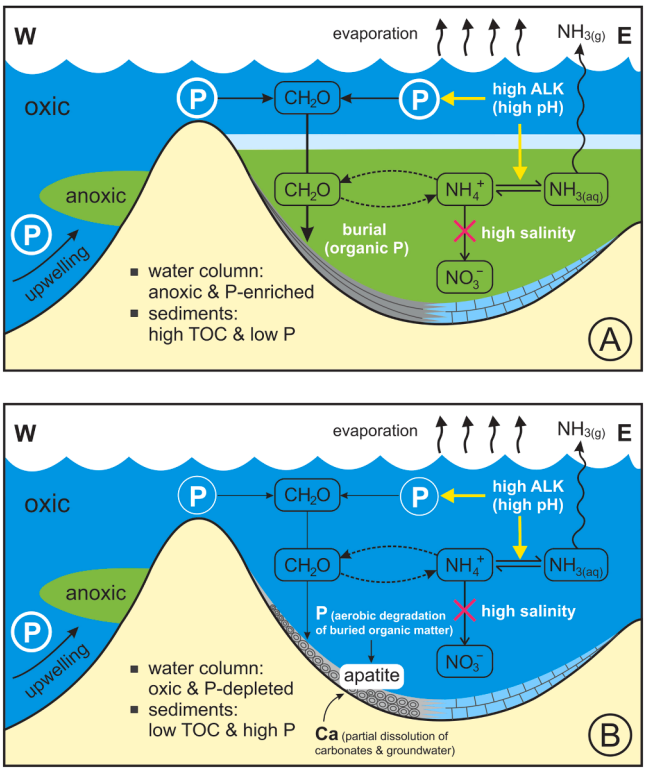

Fig. 5. Schematic representation of the evolution of marine chemistry, nitrogen and phosphorus cycling within the Phosphoria Basin. (A) The first stage with PO_4^{3-} buildup in the anoxic water column and relatively limited P burial in sediments. (B) The second stage with PO_4^{3-} depletion in the oxic water column and P enrichments (phosphogenesis) in sediments. ALK = alkalinity.

6. Concluding remarks

Taken together, our study underscores the importance of local factors—specifically alkalinity, evaporation, and basin restriction—in driving phosphogenesis within the Phosphoria Formation. These new insights may also be extended to other P-rich sedimentary sequences in Earth's history, particularly those of the Paleoproterozoic and Neoproterozoic, both of which are marked by extensive phosphatic deposits (Papineau et al., 2010). Notably, these intervals coincided with episodes of supercontinent breakup, which created numerous rift basins with variable connectivity to the open ocean. Weathering of surrounding mafic rocks could have supplied solutes that drove distinctive basin chemistries, namely elevated alkalinity. Thus, our model, which emphasizes the role of local controls, may help explain the temporal clustering of phosphorites in the geologic record. If so, it would imply that phosphorite occurrence is more closely related to Earth's tectonic evolution (e.g., the development of rift basins with locally alkaline

conditions) than to marine nutrient inventory. Further work on Precambrian phosphorites can test this hypothesis. We note, for instance, that elevated $\delta^{15}N$ (> +20‰) in shales of the phosphorite-containing Paleoproterozoic Jhamarkotra Formation (Papineau et al., 2009) might similarly reflect high alkalinity in the Aravalli Epeiric Sea.

Beyond Earth history, our findings also carry implications for astrobiology. As a fundamental component of cell membranes, genetic material, and cellular energy transfer molecules, P is central to the origin and evolution of life (Westheimer, 1987), yet in most modern environments it is a limiting nutrient. Our results demonstrate that under specific local conditions—even in the midst of the productive Phanerozoic biosphere—bioavailable PO_4^{3-} can accumulate in aqueous environments, thus providing insights into the environments that may have favored availability of P during life's emergence on Earth (Toner and Catling, 2020) and potentially on other habitable worlds.

CRediT authorship contribution statement

Chenyi Tu: Writing – original draft, Visualization, Conceptualization. **Jana Meixnerova:** Investigation. **Brett Smith:** Investigation. **Eva E. Stüeken:** Writing – review & editing. **Roger Buick:** Writing – review & editing, Conceptualization. **Christopher J. Tino:** Writing – review & editing. **Michael A. Kipp:** Writing – review & editing, Methodology, Conceptualization.

Declaration of competing interest

The authors declare that they have no known competing financial interests or personal relationships that could have appeared to influence the work reported in this paper.

Acknowledgments

We are grateful to Editor Tristan Horner and two anonymous reviewers for their constructive comments, which improved the final product. We thank Robert Hill for helpful discussions during the preparation of this manuscript. CT acknowledges support by an appointment (affiliated at Duke University) to the NASA Postdoctoral Program from the NASA Astrobiology Program, administered by Oak Ridge Associated Universities, under contract with NASA. This work was also supported by a Doctoral New Investigator award (67594-DNI2) from the American Chemical Society Petroleum Research Fund, an NSF CAREER award (OCE-2441483), and start-up funds (provided by Duke University) to MAK. RB and JM acknowledge support from the NASA Virtual Planetary Laboratory.

Supplementary materials

Supplementary material associated with this article can be found, in the online version, at doi:10.1016/j.epsl.2026.120180.

Data availability

All data are provided in the Supplementary Materials.

References

Algeo, T.J., Ingall, E., 2007. Sedimentary C_{org}: p ratios, paleocean ventilation, and phanerozoic atmospheric pO_2. Palaeogeogr. Palaeoclimatol. Palaeoecol 256, 130–155. https://doi.org/10.1016/j.palaeo.2007.02.029.

Algeo, T.J., Meyers, P.A., Robinson, R.S., Rowe, H., Jiang, G.Q., 2014. Icehouse–greenhouse variations in marine denitrification. Biogeosciences 11, 1273–1295. https://doi.org/10.5194/bg-11-1273-2014, 2014.

Algeo, T.J., Lyons, T.W., 2006. Mo–total organic carbon covariation in modern anoxic marine environments: implications for analysis of paleoredox and paleohydrographic conditions. Paleoceanography 21 (PA1016). https://doi.org/10.1029/2004PA001112.

Z.S. Altschuler, R.S. Clarke Jr., E.J. Young, "Geochemistry of uranium in apatite and phosphorite" (US Geol. Surv. Prof. Pap., 314-D, 45–90, 1958).

Bau, M., Dulski, P., 1996. Distribution of yttrium and rare-earth elements in the Penge and Kuruman iron-formations, Transvaal Supergroup, South Africa. Precambrian Res. 79, 37–55. https://doi.org/10.1016/0301-9268(95)00087-9.

Bennett, W.W., Canfield, D.E., 2020. Redox-sensitive trace metals as paleoredox proxies: a review and analysis of data from modern sediments. Earth Sci. Rev. 204, 103175. https://doi.org/10.1016/j.earscirev.2020.103175.

Bjerrum, C.J., Canfield, D.E., 2002. Ocean productivity before about 1.9 gyr ago limited by phosphorus adsorption onto iron oxides. Nature 417, 159–162. https://doi.org/10.1038/417159a.

Blättler, C.L., Higgins, J.A., 2014. Calcium isotopes in evaporites record variations in phanerozoic seawater SO_4 and Ca. Geology 42, 711–714. https://doi.org/10.1130/G35721.1.

Bushinski, G.I., 1964. On shallow water origin of phosphorite sediments. In: Developments in Sedimentology, 1. Elsevier, pp. 62–70. https://doi.org/10.1016/S0070-4571(08)70468-0.

Christ, N., Immenhauser, A., Wood, R.A., Darwich, K., Niedermayr, A., 2015. Petrography and environmental controls on the formation of phanerozoic marine carbonate hardgrounds. Earth-Sci. Rev. 151, 176–226. https://doi.org/10.1016/j.earscirev.2015.10.002.

Collister, J.W., Hays, J.M., 1973. A preliminary study of carbon and nitrogen isotopic biogeochemistry of lacustrine sedimentary rocks from the Green River Formation. In: Tuttle, M.L. (Ed.), Geochemical, Biogeochemical, and Sedimentological Studies of the Green River Formation, Wyoming, Utah, and Colorado. U.S. Geol. Surv., Denver, Wyoming, Utah, and Colorado, pp. 265–276.

Crafford, A.E.J., 2008. Paleozoic tectonic domains of Nevada: an interpretive discussion to accompany the geologic map of Nevada. Geosphere 4, 260. https://doi.org/10.1130/GES00108.1.

Crémière, A., Tino, C.J., Pommer, M.E., Cui, X., Roychowdhury, M., Summons, R.E., Sessions, A., Sarg, J.F., Lyons, T.W., Adkins, J.F., 2024. A volatile sulfur sink aids in reconciling the sulfur isotope mass balance of closed basin lakes. Geochim. Cosmochim. Acta 369, 196–212. https://doi.org/10.1016/j.gca.2024.01.008.

Dahl, T.W., Hammarlund, E.U., Anbar, A.D., Bond, D.P., Gill, B.C., Gordon, G.W., Knoll, A.H., Nielsen, A.T., Schovsbo, N.H., Canfield, D.E., 2010. Devonian rise in atmospheric oxygen correlated to the radiations of terrestrial plants and large predatory fish. Proc. Natl. Acad. Sci 107, 17911–17915. https://doi.org/10.1073/pnas.1011287107.

Davydov, V.I., Crowley, J.L., Schmitz, M.D., Snyder, W.S., 2018. New U-Pb constraints identify the end-guadalupian and possibly end-lopingian extinction events conceivably preserved in the passive margin of North America: implication for regional tectonics. Geol. Mag. 155, 119–131. https://doi.org/10.1017/S0016756816000959.

Derry, L.A., 2015. Causes and consequences of mid-proterozoic anoxia. Geophys. Res. Lett. 42, 8538–8546. https://doi.org/10.1002/2015GL065333.

Dzombak, R.M., Sheldon, N.D., 2022. Terrestrial records of weathering indicate three billion years of dynamic equilibrium. Gondwana Res 109, 376–393. https://doi.org/10.1016/j.gr.2022.05.009.

Filippelli, G.M., Delaney, M.L., 1992. Similar phosphorus fluxes in ancient phosphorite deposits and a modern phosphogenic environment. Geology 20, 709–712. https://doi.org/10.1130/0091-7613(1992)020<0709:SPFIAP>2.3.CO;2.

Föllmi, K.B., 2016. Sedimentary condensation. Earth-Sci. Rev. 152, 143–180. https://doi.org/10.1016/j.earscirev.2015.11.016.

Föllmi, K.B., Garrison, R.E., Ramirez, P.C., Zambrano-Ortiz, F., Kennedy, W.J., Lehner, B. L., 1992. Cyclic phosphate-rich successions in the upper Cretaceous of Colombia. Palaeogeogr. Palaeoclimatol. Palaeoecol. 93, 151–182. https://doi.org/10.1016/0031-0182(92)90095-M.

Geslin, J.K., 1998. Distal ancestral Rocky Mountains tectonism: evolution of the pennsylvanian-permian Oquirrh–Wood River basin, southern Idaho. Geol. Soc. Am. Bull. 110, 644–663. https://doi.org/10.1130/0016-7606(1998)110<0644:DARMTE>2.3.CO;2.

Glenn, C.R., Föllmi, K.B., Riggs, S.R., Baturin, G.N., Grimm, K.A., Trappe, J., Abed, A.M., Galli-Oliver, C., Garrison, R.E., Ilyan, A., Jehl, C., Rohrlich, V., Sadaqah, R.M., Schidlowski, M., Sheldon, R.E., Siegmund, H., 1994. Phosphorus and phosphorites: sedimentology and environments of formation. Eclogae geol. Helv. 87, 747–788.

Haas, S., Tutolo, B.M., Catling, D.C., 2025. Soda lake phosphorus fluxes controlled by biological uptake imply abundant phosphate in plausible origin-of-life environments. Geochim. Cosmochim. Acta 393, 63–74. https://doi.org/10.1016/j.gca.2025.01.040.

Hayes, J.M., Kaplan, I.R., Wedeking, K.W., 1983. Precambrian organic geochemistry, preservation of the record". In: Schopf, J.W. (Ed.), Earth's Earliest Biosphere–Its Origin and Evolution. Princeton University Press, Princeton, NJ, pp. 93–134.

Hein, J.R., Perkins, R.B., McIntyre, B.R., 2004. Evolution of thought concerning the origin of the Phosphoria Formation, western US phosphate field. In: Handbook of Exploration and Environmental Geochemistry, 8. Elsevier, pp. 19–42. https://doi.org/10.1016/S1874-2734(04)80004-4.

Hiatt, E.E., 1997. A Paleoceanographic Model for Oceanic Upwelling in a Late Paleozoic Epicontinental sea: a Chemostratigraphic Analysis of the Permian Phosphoria Formation. University of Colorado, Boulder, CO thesis.

Hiatt, E.E., Budd, D.A., 2001. Sedimentary phosphate formation in warm shallow waters: new insights into the palaeoceanography of the Permian Phosphoria Sea from analysis of phosphate oxygen isotopes. Sediment. Geol. 145, 119–133. https://doi.org/10.1016/S0037-0738(01)00127-0.

Hill, R.C., Wang, Z., Williams, G.D., Polyak, V., Singh, A., Kipp, M.A., Asmerom, Y., Vengosh, A., 2024. Reconstructing the depositional environment and diagenetic modification of global phosphate deposits through integration of uranium and

strontium isotopes. Chem. Geol. 662, 122214. https://doi.org/10.1016/j.chemgeo.2024.122214.
Hite, R.J., 1978. Possible genetic relationships between evaporites, phosphorites, and iron-rich sediments. Mt. Geol. 14, 97–107.
Ilyin, A.V., 1998. Rare-earth geochemistry of 'old' phosphorites and probability of syngenetic precipitation and accumulation of phosphate. Chem. Geol. 144, 243–256. https://doi.org/10.1016/S0009-2541(97)00134-4.
Ingall, E., Jahnke, R., 1994. Evidence for enhanced phosphorus regeneration from marine sediments overlain by oxygen depleted waters. Geochim. Cosmochim. Acta 58, 2571–2575. https://doi.org/10.1016/0016-7037(94)90033-7.
Ingalls, M., Grotzinger, J.P., Present, T., Rasmussen, B., Fischer, W.W., 2022. Carbonate-associated phosphate (CAP) indicates elevated phosphate availability in Neoarchean shallow marine environments. Geophys. Res. Lett. 49. https://doi.org/10.1029/2022GL098100 e2022GL098100.
Keighley, D., 2015. Phosphatic carbonate shale of the 'bird's Nest saline zone', Upper Green River Formation, Uinta Basin, Utah. In: Smith, M., Carroll, A. (Eds.), Stratigraphy and Paleolimnology of the Green River Formation, Western USA, 1. Springer, Dordrecht, pp. 251–276. https://doi.org/10.1007/978-94-017-9906-5_10.
Kipp, M.A., Stüeken, E.E., Yun, M., Bekker, A., Buick, R., 2018. Pervasive aerobic nitrogen cycling in the surface ocean across the paleoproterozoic era. Earth Planet. Sci. Lett. 500, 117–126. https://doi.org/10.1016/j.epsl.2018.08.007.
Kluth, C.F., Coney, P.J., 1981. Plate tectonics of the ancestral Rocky Mountains. Geology 9, 10–15. https://doi.org/10.1130/0091-7613(1981)9<10:PTOTAR>2.0.CO;2.
Li, L., Lollar, B.S., Li, H., Wortmann, U.G., Lacrampe-Couloume, G., 2012. Ammonium stability and nitrogen isotope fractionations for NH_4^+–$NH_{3(aq)}$–$NH_{3(gas)}$ systems at 20–70 °C and pH of 2–13: applications to habitability and nitrogen cycling in low-temperature hydrothermal systems. Geochim. Cosmochim. Acta 84, 280–296. https://doi.org/10.1016/j.gca.2012.01.040.T.
Lowenstein, K., Timofeeff, M.N., Brennan, S.T., Hardie, L.A., Demicco, R.V., 2001. Oscillations in phanerozoic seawater chemistry: evidence from fluid inclusions. Science 294, 1086–1088. https://doi.org/10.1126/science.1064280.
Li, X., Hu, Y., Guo, J., Lan, J., Lin, Q., Bao, X., Yuan, S., Wei, M., Li, Z., Man, K., Yin, Z., 2022. A high-resolution climate simulation dataset for the past 540 million years. Sci. Data 9, 371. https://doi.org/10.1038/s41597-022-01490-4.
Lipp, A.G., Shorttle, O., Sperling, E., Brocks, J.J., Cole, D., Crockford, P.W., Del Mouro, L., Dewing, K., Dornbos, S.Q., Emmings, J.F., 2021. The composition and weathering of the continents over geologic time. Geochem. Perspect. Lett. 17, 21–26. https://doi.org/10.7185/geochemlet.2109.
Lowenstein, T.K., Jagniecki, E.A., Carroll, A.R., Smith, M.E., Renaut, R.W., Owen, R.B., 2017. The Green River salt mystery: what was the source of the hyperalkaline lake waters? Earth-Sci. Rev. 173, 295–306. https://doi.org/10.1016/j.earscirev.2017.07.014.
Marshall, M.S., 2025. Skeletal concentrations in upwelling records: greater sensitivity to hiatal duration than to paleo-oxygenation in the Permian Phosphoria Rock Complex. Palaeogeogr. Palaeoclimatol. Palaeoecol. 675, 113084. https://doi.org/10.1016/j.palaeo.2025.113084.
Maughan, E.K., 1994. Phosphoria Formation and its resource significance in the western interior, USA. In: Embry, A.F., Beauchamp, B., Glass, D.J. (Eds.), Pangea: Global Environments and Resources. Canadian Society of Petroleum Geologists Memoir, Calgary, pp. 479–495. Memoir 17.
Matheson, E.J., Frank, T.D., 2020. Phosphorites, glass ramps and carbonate factories: the evolution of an epicontinental sea and a late palaeozoic upwelling system (Phosphoria Rock Complex). Sedimentology 67, 3003–3041. https://doi.org/10.1111/sed.12731.
McKelvey, V.E., Cheney, T.M., Cressman, E.R., Sheldon, R.P., Swanson, R.W., Williams, J.S., 1959. The Phosphoria, Park City, and Shedhorn formations in the western phosphate field. US Geol. Surv. Prof. Pap. 313-A, 1–47.
Papineau, D., 2010. Global biogeochemical changes at both ends of the Proterozoic: insights from phosphorites. Astrobiology 10, 165–181. https://doi.org/10.1089/ast.2009.0360.
Papineau, D., Purohit, R., Fogel, M.L., Shields-Zhou, G.A., 2013. High phosphate availability as a possible cause for massive cyanobacterial production of oxygen in the paleoproterozoic atmosphere. Earth Planet Sci. Lett. 362, 225–236. https://doi.org/10.1016/j.epsl.2012.11.050.
Papineau, D., Purohit, R., Goldberg, T., Pi, D., Shields, G.A., Bhu, H., Steele, A., Fogel, M.L., 2009. High primary productivity and nitrogen cycling after the paleoproterozoic phosphogenic event in the Aravalli Supergroup, India. Precambrian Res. 171, 37–56. https://doi.org/10.1016/j.precamres.2009.03.005.
R.B. Perkins, B. McIntyre, J.R. Hein, D.Z. Piper, "Geochemistry of permian rocks from the margins of the Phosphoria Basin: lakeridge core, western Wyoming" (US Geol. Surv., Open-File Rep., 2003-21, 2003). https://doi.org/10.3133/ofr0321.
Piper, D.Z., 2001. Marine chemistry of the Permian Phosphoria Formation and basin, southeast Idaho. Econ. Geol. 96, 599–620. https://doi.org/10.2113/gsecongeo.96.3.599.
Pommer, M., Sarg, J.F., 2019. Biochemical and stratigraphic controls on pore-system evolution, Phosphoria Rock Complex (Permian), Rocky Mountain Region, USA. In: McNeill, D.F., Harris, P., Rankey, E.C., Hsieh, J.C.C. (Eds.), Carbonate Pore Systems: New Developments and Case Studies, 112. SEPM. https://doi.org/10.2110/sepmsp.112.13.
Pufahl, P.K., Groat, L.A., 2017. Sedimentary and igneous phosphate deposits: formation and exploration: an invited paper. Econ. Geol. 112, 483–516. https://doi.org/10.2113/econgeo.112.3.483.
Raiswell, R., Hardisty, D.S., Lyons, T.W., Canfield, D.E., Owens, J.D., Planavsky, N.J., Poulton, S.W., Reinhard, C.T., 2018. The iron paleoredox proxies: a guide to the pitfalls, problems and proper practice. Am. J. Sci. 318, 491–526. https://doi.org/10.2475/05.2018.03.
Reinhard, C.T., Planavsky, N.J., Gill, B.C., Ozaki, K., Robbins, L.J., Lyons, T.W., Fischer, W.W., Wang, C., Cole, D.B., Konhauser, K.O., 2017. Evolution of the global phosphorus cycle. Nature 541, 386–389. https://doi.org/10.1038/nature20772.
Reynard, B., Lécuyer, C., Grandjean, P., 1999. Crystal-chemical controls on rare-earth element concentrations in fossil biogenic apatites and implications for paleoenvironmental reconstructions. Chem. Geol. 155, 233–241. https://doi.org/10.1016/S0009-2541(98)00169-7.
Sahoo, S.K., Gilleaudeau, G.J., Wilson, K., Hart, B., Barnes, B.D., Faison, T., Bowman, A.R., Larson, T.E., Kaufman, A.J., 2023. Basin-scale reconstruction of euxinia and late devonian mass extinctions. Nature 615, 640–645. https://doi.org/10.1038/s41586-023-05716-2.
Sandberg, P.A., 1983. An oscillating trend in phanerozoic non-skeletal carbonate mineralogy. Nature 305, 19–22. https://doi.org/10.1038/305019a0.
Scotese, C.R., 2021. An atlas of phanerozoic paleogeographic maps: the seas come in and the seas go out. Ann. Rev. Earth Planet. Sci. 49, 679–728. https://doi.org/10.1146/annurev-earth-081320-064052.
Scott, C., Lyons, T.W., 2012. Contrasting molybdenum cycling and isotopic properties in euxinic versus non-euxinic sediments and sedimentary rocks: refining the paleoproxies. Chem. Geol. 324-325, 19–27. https://doi.org/10.1016/j.chemgeo.2012.05.012.
Sheldon, R.P., 1989. Phosphorite deposits of the Phosphoria Formation, Western United States. In: Notholt, A.J.G., Sheldon, R.P., Davidson, D.F. (Eds.), Phosphate Deposits of the World, Phosphate Rock Resources, 2. Cambridge University Press, Cambridge, pp. 53–61.
W. Shepard, B. Bartow, "Tectonic history of the sweetgrass arch, a key to finding new hydrocarbons, Montana, and Alberta" (The AAPG/Datapages Combined Publications Database, Wyoming Geological Association, 9–19, 1986).
Southgate, P.N., 1980. Cambrian stromatolitic phosphorites from the Georgina Basin, Australia. Nature 285, 395–397. https://doi.org/10.1038/285395a0.
Stephens, N.P., Carroll, A.R., 1999. Salinity stratification in the Permian Phosphoria sea; a proposed paleoceanographic model. Geology 27, 899–902. https://doi.org/10.1130/0091-7613(1999)027<0899:SSITPP>2.3.CO;2.
Stüeken, E.E., Buick, R., Schauer, A.J., 2015. Nitrogen isotope evidence for alkaline lakes on late archean continents. Earth Planet. Sci. Lett. 411, 1–10. https://doi.org/10.1016/j.epsl.2014.11.037.
Stüeken, E.E., Kipp, M.A., Koehler, M.C., Buick, R., 2016. The evolution of Earth's biogeochemical nitrogen cycle. Earth Sci. Rev. 160, 220–239. https://doi.org/10.1016/j.earscirev.2016.07.007.
Stüeken, E.E., Tino, C., Arp, G., Jung, D., Lyons, T.W., 2020. Nitrogen isotope ratios trace high-pH conditions in a terrestrial Mars analog site. Sci. Adv. 6. https://doi.org/10.1126/sciadv.aay3440 eaay3440.
Stüeken, E.E., Zaloumis, J., Meixnerová, J., Buick, R., 2017. Differential metamorphic effects on nitrogen isotopes in kerogen extracts and bulk rocks. Geochim. Cosmochim. Acta 217, 80–94. https://doi.org/10.1016/j.gca.2017.08.019.
Sweere, T., van den Boorn, S., Dickson, A.J., Reichart, G.J., 2016. Definition of new trace-metal proxies for the controls on organic matter enrichment in marine sediments based on Mn, Co, Mo and Cd concentrations. Chem. Geol. 441, 235–245. https://doi.org/10.1016/j.chemgeo.2016.08.028.
Tesdal, J.E., Galbraith, E.D., Kienast, M., 2013. Nitrogen isotopes in bulk marine sediment: linking seafloor observations with subseafloor records. Biogeosciences 10, 101–118. https://doi.org/10.5194/bg-10-101-2013.
Tino, C.J., Stüeken, E.E., Gregory, D.D., Lyons, T.W., 2025. Elevated $\delta^{15}N$ linked to inhibited nitrification coupled to ammonia volatilization in sediments of shallow alkaline-hypersaline lakes. Geobiology 23, e70018. https://doi.org/10.1111/gbi.70018.
Toner, J.D., Catling, D.C., 2020. A carbonate-rich lake solution to the phosphate problem of the origin of life. Proc. Natl. Acad. Sci. U.S.A. 117, 883–888. https://doi.org/10.1073/pnas.1916109117.
Tosca, N.J., Tutolo, B.M., 2023. How to make an alkaline lake: fifty years of chemical divides. Elements 19, 15–21. https://doi.org/10.2138/gselements.19.1.15.
Tostevin, R., 2021. Cerium anomalies and paleoredox. In: Lyons, T.W., Turchyn, A.V., Reinhard, C.T. (Eds.), Elements in Geochemical Tracers in Earth System. Cambridge University Press. https://doi.org/10.1017/9781108847223.
Tostevin, R., Wood, R.A., Shields, G.A., Poulton, S.W., Guilbaud, R., Bowyer, F., Penny, A.M., He, T., Curtis, A., Hoffmann, K.H., Clarkson, M.O., 2016. Low-oxygen waters limited habitable space for early animals. Nat. Commun. 7, 12818. https://doi.org/10.1038/ncomms12818.
Tyrrell, T., 1999. The relative influences of nitrogen and phosphorus on oceanic primary production. Nature 400, 525–531. https://doi.org/10.1038/22941.
Velazquez, D., Sheldon, N.D., Hren, M.T., Kharbush, J.J., 2025. Oxygenation and alkalinity drive the lacustrine nitrogen isotope record throughout the past 3.2 billion years. Geobiology 23, e70033. https://doi.org/10.1111/gbi.70033.
Wardlaw, B.R., 2015. Gondolellid conodonts and depositional setting of the Phosphoria Formation. Micropaleontology 61, 335–368. https://www.jstor.org/stable/44511382.
Westheimer, F.H., 1987. Why nature chose phosphates. Science 235, 1173–1178. https://doi.org/10.1126/science.2434996.
Zhao, Y., Wei, W., Li, S., Yang, T., Zhang, R., Somerville, I., Santosh, M., Wei, H., Wu, J., Yang, J., Chen, W., Tang, Z., 2021. Rare earth element geochemistry of carbonates as a proxy for deep-time environmental reconstruction. Palaeogeogr. Palaeoclimatol. Palaeoecol. 574, 110443. https://doi.org/10.1016/j.palaeo.2021.110443.